Accepted manuscript (author version)

To appear in:
International Journal of Nano Dimension (Int. J. Nano Dimens.)

Online ISSN: 2228-5059 Print ISSN: 2008-8868

Dates:
Received: 16 October 2025
Revised: 22 November 2025
Accepted: 05 December 2025

DOI: https://doi.org/10.57647/ijnd.2026.1703.02

Time-Controlled Photoassisted Deposition of Silver on Tio2 Nanotube Arrays: Tuning Plasmonic for Enhanced Photoelectrochemical Performance

Qasim Chfat Abdulridha [1], Araa Mebdir Holi [1,*], Azhar Y.M. Al-Murshedi [2]

[1] *Department of Physics, College of Education, University of Al-Qadisiyah, Al-Diwaniyah, Al-Qadisiyah 58002, Iraq*
[2] *Chemistry Department, Faculty Education for Women, University of Kufa, Najaf, Iraq*

**Corresponding author. E-mail:* araa.holi@qu.edu.iq

Abstract

This study demonstrates that time-controlled photoassisted deposition of silver (Ag) nanoparticles can effectively tune the plasmonic and photoelectrochemical behavior of TiO_2 nanotube arrays (TNTs/Ti foil). Structural analyses confirmed the preservation of phase-pure anatase TiO_2 and revealed progressive Ag loading with deposition time. FESEM observations showed that early deposition (5–15 min) primarily thickened tube walls, increasing the outer diameter from ~210 to ~250 nm, while distinct Ag nanoparticles were not yet resolved. At longer deposition times (20–25 min), well-defined Ag particles appeared, growing from ~450 to ~750 nm, indicating coalescence and aggregation. These morphological changes corresponded with optical responses, where a pronounced LSPR band emerged at ~620 nm and the apparent band gap decreased from 3.20 eV for pristine TNTs to 2.7 eV at 10 min Ag coverage. Photoelectrochemical measurements highlighted the importance of deposition time: photocurrent density increased from 0.11 mA cm^{-2} for pristine TNTs to a maximum of 0.39 mA cm^{-2} at 10 min, over 3.5-fold enhancement, before declining due to aggregation-induced recombination. Overall, these results show that precise control of Ag deposition time governs nanoparticle nucleation, growth, plasmonic behavior, and interfacial charge transfer, providing a scalable strategy for designing high-performance plasmonic photoelectrodes.

Keywords: *Photoassisted deposition; Photoelectrochemical performance; Plasmonic effect; Silver nanoparticles; Surface modification; TiO_2 nanotubes.*

1. Introduction

Over the past decade, nanoscale semiconductor structures have attracted significant interest due to their potential in advanced optoelectronic and photoelectrochemical applications. Numerous studies have explored different fabrication strategies to enhance structural uniformity, optical absorption, and interfacial charge transfer, all of which are crucial for improving energy conversion efficiency [1–6]. Within this context, TiO_2 nanotube arrays (TNTAs) have gained particular attention because of their well-ordered morphology, high surface area, and efficient one-dimensional electron transport pathways [7-9]. These properties make TNTAs promising photoanodes for solar-driven PEC systems [10]. However, the wide band gap of TiO_2 (~3.2 eV) restricts its activity to the UV region, which represents a small fraction of the solar spectrum. Various modification strategies such as coupling with narrow-band-gap semiconductors (e.g., CdS) or controlling electrolyte composition during nanotube formation have been shown to improve visible-light response and interfacial charge dynamics [11-12]. Despite these advances, noble-metal decoration, particularly with silver (Ag), remains one of the most effective methods for enhancing visible-light absorption through localized surface plasmon resonance (LSPR) [13]. Noble metals such as Pt, Au, Ag, and Pd generate strong electromagnetic fields at the metal–semiconductor interface, boosting photon harvesting and suppressing charge recombination [14-17].

Ag nanoparticles are especially attractive due to their tunable plasmonic properties and strong surface plasmon resonance in the UV–visible range [18, 19]. Integrating Ag with TiO_2 leads to broadened optical absorption, enhanced charge separation, and improved PEC activity under both UV and visible illumination, as widely demonstrated in plasmon-enhanced TiO_2 systems

[20-22]. Previous studies further show that Ag decoration can introduce defect states, modify band alignment, and significantly enhance photocatalytic and PEC performance [23, 24]. Although Ag-modified TiO_2 nanotubes have been widely studied using photoreduction, chemical reduction, and electrodeposition, the literature still lacks a systematic investigation of how precisely controlled photoassisted deposition time dictates Ag loading, plasmonic behavior, band-edge alignment, and the resulting PEC performance. This gap highlights the need for time-resolved deposition studies, which the present work directly addresses. Recent studies have extensively explored noble-metal modification of TiO_2 nanostructures, particularly Ag, to boost photoelectrochemical (PEC) performance. Although various methods including photoreduction, chemical reduction, and electrodeposition have been used to improve light absorption, plasmonic response, and charge separation, the literature still lacks a systematic understanding of how precisely controlled photodeposition time governs the evolution of Ag nanoparticle loading, band-edge alignment, and the resulting PEC behavior. Prior reports have only addressed isolated aspects of this relationship. For instance, Liu et al. (2019) [25] demonstrated that electrodeposition followed by H/N post-treatment produces Ag/TiO_{2-x} nanotubes with significantly enhanced photocurrent and plasmonic response due to oxygen-vacancy formation and improved electron transport, while Zhang et al. (2020) [26] highlighted that the metal-deposition sequence alters the LSPR response. Likewise, a study in Veziroglu et al. (2024) [27] reported that the sequence and duration of photodeposition of Ag and Au nanoparticles critically govern the resulting plasmonic resonance, spectral tunability, and PEC behavior of TiO_2 nanotube arrays. Additional studies, including Yang et al. (2021) [28] and Chen et al. (2022) [29], confirm the importance of controlled Ag loading but do not establish a quantitative link between deposition time, structural evolution, and PEC performance. Photo-deposition was

employed to decorate Ag nanoparticles on TiO_2 nanotubes due to its ability to drive site-selective nucleation via photogenerated electrons, ensuring strong interfacial contact and efficient charge separation. Unlike conventional chemical reduction, sol-gel, or SILAR methods, which often lead to random particle deposition and aggregation, photo-deposition provides precise control over particle size, distribution, and coverage. The approach is also milder, cleaner, and environmentally friendly, making it ideal for fabricating highly efficient Ag- TiO_2 nanotube photoelectrodes.

In this context, the present work addresses this gap by systematically correlating photoassisted Ag deposition duration with the resulting structural, optical, and PEC properties of TiO_2 nanotube arrays. By resolving how deposition time modulates PEC performance, this study provides a clearer design framework for optimizing Ag- TiO_2 interfaces and advancing next-generation PEC systems for solar-driven applications.

2. Experimental

Titanium dioxide (TiO_2) nanotube arrays were fabricated via the anodization technique. Titanium foils (99.9% purity, Sigma-Aldrich) were cut into rectangular pieces of 2.5 × 1.0 cm^2 and sequentially ultrasonicated for 15 minutes in acetone, isopropanol, and deionized water to remove organic contaminants. Subsequently, the foils were immersed in 6 M HNO_3 for 10 minutes to eliminate surface impurities and obtain a smooth, clean surface. An electrochemical cell was assembled, where the titanium foil served as the working electrode and a high-density graphite plate acted as the counter electrode. The inter-electrode distance was maintained at 2 cm. Anodization was conducted using a DC power supply (MP6010D) in an electrolyte containing 75 mL glycerin, 25 mL deionized water, and 0.5 g ammonium fluoride (NH_4F), as illustrated in Figure 1.

Following anodization, the resulting TiO_2 films were annealed in air at 500 °C for 2 hours to obtain well-crystallized TiO_2 nanotube arrays. Photodeposition method employing a mercury UV lamp (365 nm, 300 W) providing an irradiance of approximately 150 mW/cm² at a distance of 10 cm from the sample surface. The photodeposition was carried out at a controlled temperature of 27°C within the deposition chamber. The temperature was maintained by employing a vacuum exhaust system to remove the hot air generated by the UV lamp and prevent overheating of the sample. The TiO_2 nanotube arrays grown on Ti foils were used as substrates, and photodeposition was performed in an aqueous 0.1 M $AgNO_3$ solution for different irradiation times (5, 10, 15, 20, and 25 minutes). After photodeposition, the samples were thoroughly rinsed with deionized water and dried at room temperature, as schematically presented in Figure 1. Under UV illumination, photogenerated electrons from TiO_2 reduce Ag^+ ions to metallic Ag, leading to nucleation and growth of Ag nanoparticles directly on the nanotube surface, while holes oxidize residual species in the solution. The deposition time was adjusted to control particle size and surface coverage.

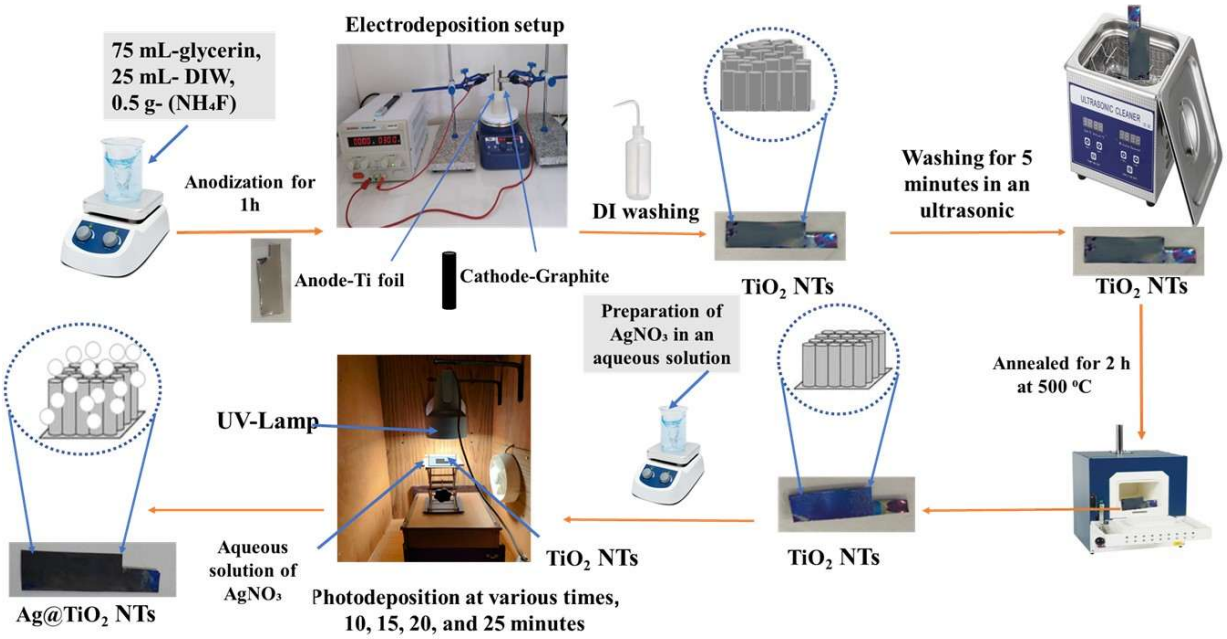

Figure 1. Schematic diagram of the synthesis of Ag@TiO_2 NTs.

2.1 Characterization of TiO_2 nanotubes

The X-ray diffraction (XRD) evaluation was accomplished using the Shimadzu LabX XRD-6000 diffractometer, which operated inside a scanning variety of 10º to 80º using Cu Kα radiation (λ = 1.54 Å). The instrument was changed into a set to a working voltage of 40. kV and a current of 40 mA. Morphological characterization of the samples was carried out using field-emission scanning electron microscopy (FESEM, Nova Nano SEM 450), while elemental composition and distribution were analyzed by energy-dispersive X-ray spectroscopy (EDS) attached to the same instrument. UV-visible diffuse reflectance spectroscopy was performed using the Shimadzu TM DUV 3700 double-beam spectrophotometer, covering a wavelength variety from 200 to 800 nm. For PEC studies, a conventional three-electrode electrochemical cell was employed to evaluate the performance of TiO_2 and Ag@ TiO_2 nanotube (NT) electrodes. The TiO_2 and Ag@ TiO_2 NT samples were used as working electrodes, with a silver/silver chloride (Ag/AgCl) electrode as the reference and a platinum (Pt) wire as the counter electrode. The electrolyte solution consisted of

0.1 M Na_2S and 0.1 M Na_2SO_3, adjusted to a pH of ~13. Photocurrent measurements were performed using linear sweep voltammetry (LSV) with a Vertex One potentiostat (Ivium Technologies, Netherlands) controlled by IviumSoft software. The potential was swept from –1.0 V to +1.0 V versus Ag/AgCl at a scan rate of 20 mV/s. A 300 W halogen lamp (120 V) served as the light source, positioned 15 cm from the quartz reaction cell, providing an illumination intensity of ~100 mW/cm² over an active electrode area of 1 cm². The light was modulated manually (chopped) to record photocurrent responses under intermittent illumination. The applied bias photon-to-current efficiency (ABPE) was calculated using the following relation [30]:

$$\eta = \frac{J_{ph}\left(E^{o}_{rev} - \left|E_{app.}\right|\right)}{P_{in}} \times 100\% \qquad (1)$$

P_{in} is the incident light irradiance (100 mWcm^{-2}), and J_{ph} ($J_{ph} = J_L - J_D$) denotes the achieved photocurrent density (in mAcm^{-2}) under the externally applied voltage of V_{app} *vs.* Ag/AgCl. E_{app} denotes the standard reversible potential, which is 1.23 V vs. the normal hydrogen electrode (NHE), and E_{app} is the actual electrode potential between the working electrode and the counter electrode at which the photocurrent was measured under illumination.

3. Results and discussion

3.1 XRD analysis

The crystalline structures of the anodized TiO_2 nanotube arrays and silver-decorated TiO_2 nanotubes (Ag@TiO_2 NTs) prepared via photodeposition for varying durations (5, 10, 15, 20, and 25 minutes) were analyzed using X-ray diffraction (XRD). The obtained diffraction patterns were compared systematically with standard reference data from the Joint Committee on Powder

Diffraction Standards (JCPDS): metallic titanium (Ti, card no. 00-044-1294), anatase TiO_2 (card no. 00-021-1272), and metallic silver (Ag, card nos. 00-004-0783). As shown in Figure 2, the XRD pattern of the pristine titanium substrate exhibited characteristic diffraction peaks at 2θ values of approximately 35.42°, 38.60°, 40.44°, 53.52°, 63.15°, 70.80°, and 76.41°, which correspond to the (100), (002), (101), (102), (103), (112), and (201) crystallographic planes of metallic Ti, respectively. Following an oxidative preparation of 1 hour (designed as TNT), new diffraction peaks emerged at 2θ values near 25.11°, 38.23°, 47.86°, and 52.86°, as a result of the anatase phase of TiO_2 with planes (100), (004), (200), and (105). Notably, the (100) anatase peak at ~25.3° was particularly intense, indicating a preferential orientation and more suitable crystallinity of regular anatase TiO_2 with thermodynamically favorable successful alongside this plane. The attenuation of Ti peaks expanded anatase depth, indicating the formation alongside of an extra uniform and thicker TiO_2 nanotube layer oxidation, with the average crystallite size expected at approximately 22.1 nm via Scherrer's equation. These effects are in agreement with earlier studies [31–33]. The subsequent deposition of silver led to additional diffraction reflections, primarily at approximately 38.1°, 44.3°, 64.4°, and 77.3°, which correspond to the (111), (200), (220), and (311) planes of silver, respectively matching JCPDS cards 00-004-0783. These XRD peaks confirm the successful nucleation and formation of crystalline silver nanoparticles on the TiO_2 substrate. The deposition time significantly influences the nanoparticle size, crystallinity, and phase development, with longer deposition durations promoting the growth of larger and well-defined metallic silver domains. A comprehensive evaluation of the silver photodeposition intervals reveals a progressive and systematic evolution in nanoparticle growth. At the initial stage (5 min), the diffraction peaks associated with metallic silver are relatively broad with moderate intensity, indicating the onset of nucleation and the formation of

small crystallites (~23.5 nm), characteristic of the cubic phase of Ag. For Ag-10min@TNT, the increased peak intensity with slightly reduced peak broadening indicates higher Ag loading and surface coverage, while the Scherrer-estimated crystallite size (~29 nm) confirms nanoscale growth without altering the crystallinity of the TiO_2 substrate. At Ag-15min@TNT, further enhancement in peak intensity along with moderate broadening suggests continued nucleation and gradual particle growth (~29.1 nm), reflecting the stabilizing effect of extended photodeposition. In the case of Ag-20min@TNT, the sharper and more intense diffraction peaks correspond to improved crystallinity and an increase in Ag domain size (~32 nm). Finally, for Ag-25min@TNT, the most intense peaks with reduced broadening indicate substantial particle growth (~40 nm), consistent with extensive photodeposition leading to larger, well-developed Ag nanoparticles. This systematic progression underscores the critical role of deposition time in dictating nanoparticle size, crystallinity, and phase evolution. Prolonged deposition durations prefer the development of massive, strong metallic silver domain names on TiO_2 nanotubes. These findings provide valuable insights for optimizing nanocomposite fabrication strategies, with direct implications for advanced applications in photocatalysis, sensing, and antimicrobial coatings, and are in settlement with previous reports [34-37].

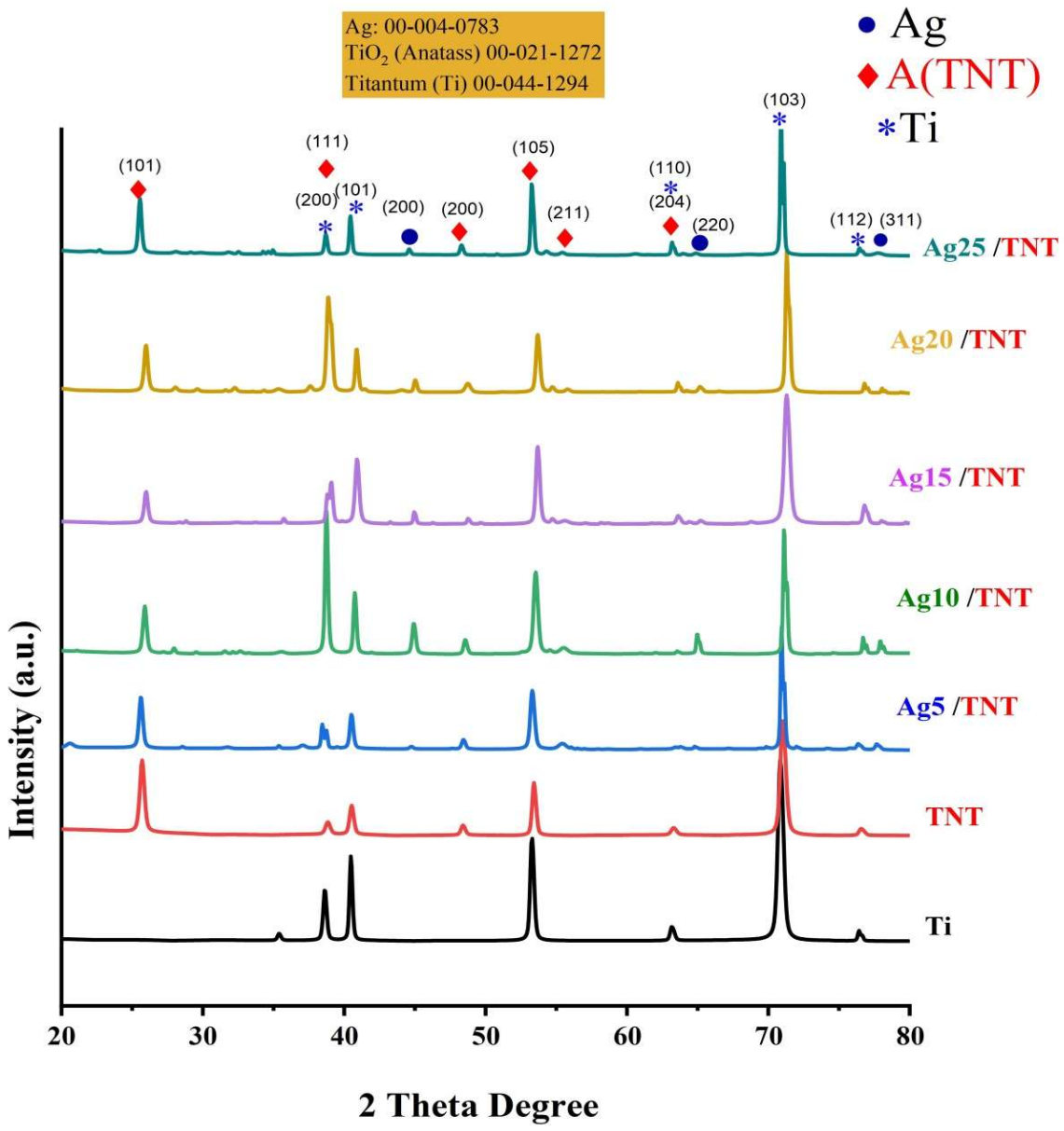

Figure 2. XRD patterns of pristine TiO_2 nanotube arrays (TNTs) and Ag-decorated TNTs obtained at various photodeposition durations.

.2 Morphological and EDS Analysis

The pristine TiO_2 nanotubes (TNTs) (Figure 3a) exhibit highly ordered and uniform nanotubular architecture with smooth walls, well-defined openings, and minimal structural defects, providing a stable platform for surface modification. The average inner diameter of the tubes is

approximately 95 nm, consistent with typical anodically grown TiO_2 nanotubes. No discrete nanoparticles are observed on the pristine surface, and the only measurable "particle-like" feature corresponds to the tube diameter with wall thickness. Upon Ag photodeposition, the morphological evolution depends strongly on deposition time (Figure 3b–f). At early stages (5–15 min) Figure 3b-d, distinct Ag nanoparticles are not yet resolved in FESEM images; instead, the outer tube diameter increases progressively from ~210 nm (5 min) to ~230 nm (10 min) and ~250 nm (15 min), reflecting partial wall thickening and early-stage nucleation. In the Ag-5min@TNTs sample, sparse Ag nuclei appear near the tube openings, indicating limited surface coverage. In contrast, by 10 min, a more uniform distribution of Ag along the tube mouth is observed, corresponding to optimally sized nanoparticles that promote enhanced plasmonic activity and efficient charge separation. At 15 min, the deposition produces a denser metallic layer, suggesting the onset of particle coalescence. At longer deposition times Figure 3e-f, discrete metallic Ag particles become clearly visible, with particle sizes increasing sharply to ~450 nm at 20 min and forming large agglomerates of ~750 nm at 25 min. These larger clusters reduce the effective active surface area of the nanotubes, induce plasmon damping, and increase light scattering, thereby adversely affecting charge transport and photoelectrochemical performance. Tube diameter and Ag particle-size estimation from Figure 3 (histograms) shows a clear growth trend with deposition time. Histogram analysis confirms this progressive particle-size evolution, from small nuclei at early stages, through uniform nanoparticles at intermediate times, to coalesced and aggregated domains at prolonged deposition. Overall, these observations highlight the critical role of Ag deposition time in tuning the morphological, optical, and photoelectrochemical properties of TiO_2 nanotube arrays. Moderate deposition (10 min) yields the most favorable balance between nanoparticle dispersion, plasmonic enhancement, and charge

separation, whereas excessive loading leads to aggregation and diminished functional performance.

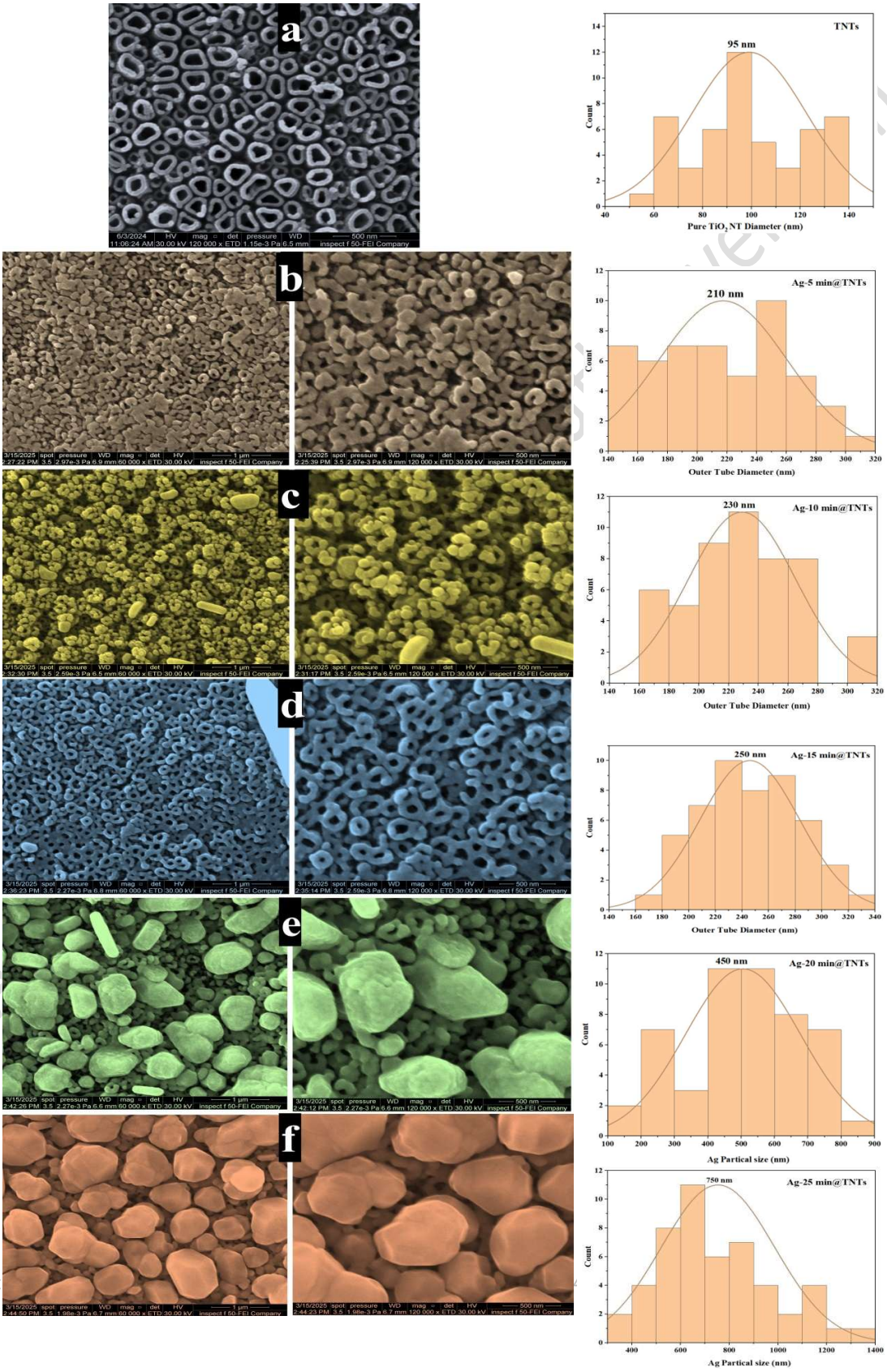

Figure 3. FESEM images at different magnifications showing the surface morphology of (a) pristine TiO_2 nanotube arrays (TNTs), and Ag-decorated TNTs obtained at various photodeposition durations: (b) Ag-5min@TNTs; (c) Ag-10min@TNTs; (d) Ag-15min@TNTs; (e) Ag-20min@TNTs; (f) Ag-25min@TNTs. Approximate particle-size histograms for TNT and Ag nanoparticles on TiO_2 nanotubes as a function of photodeposition time

Figure (4a–f) presents cross-sectional field-emission scanning electron microscopy (FESEM) images depicting the morphological evolution of TiO_2 nanotube arrays and their Ag-decorated counterparts via photodeposition at different durations.

The reference image (Figure 4a) shows pristine TiO_2 nanotubes synthesized via 1-hour anodization. The nanotubes are vertically aligned, highly ordered, and uniform in length, with well-defined smooth walls. This open, homogeneous tubular morphology confirms successful anodic formation, consistent with previous reports that optimized anodization conditions yield dense and well-established TiO_2 nanotube arrays [43]. The absence of surface particulates further validates their pristine nature, making them an ideal template for subsequent nanoparticle decoration. In Figure 4b (Ag-5min@TNT), initial Ag nucleation is observed as isolated nanoscale clusters moderately dispersed on the nanotube surfaces and within the tubular openings. This early stage of photodeposition reflects localized reduction of Ag^+ ions by photogenerated electrons (Taipina et al., 2021) [44]. The overall nanotube morphology remains largely intact, indicating minimal structural disturbance. For Figure 4c (Ag-10min@TNT), the density of Ag nanoparticles increases significantly, with uniform attachment along the inner walls and outer diameter of the nanotubes. The morphology is still predominantly unaltered, demonstrating controlled nanoparticle growth without substantial blockage of the tubular channels. In Figure 4d (Ag-15min@TNT), larger Ag nanoparticles appear, particularly along the

outer edges of the nanotubes. While the overall structure is preserved, partial particle coalescence suggests the onset of aggregation, and some obstruction of tube openings may slightly influence photocatalytic activity by modifying light absorption and site accessibility. Figure 4e (Ag-20min@TNT) shows further particle accumulation and more pronounced partial occlusion of the nanotube openings. This surface saturation aligns with literature reports indicating that excessive metal deposition can cause surface roughening and cluster formation, potentially reducing the available active surface area and affecting plasmonic resonance and photocatalytic efficiency.

Finally, Figure 4f (Ag-25min@TNT) exhibits near-complete coverage with densely aggregated Ag nanoparticles and extensive coalescence zones. Such excessive silver loading can negatively impact photocatalytic performance due to light reflection, shadowing effects, and restricted access of reactants to the nanotube interior, thereby hindering charge transfer processes. Overall, these FESEM images demonstrate that Ag nanoparticle deposition via photoreduction exhibits a clear time-dependent behavior, profoundly influencing the morphology of TiO_2 nanotubes. Optimizing deposition duration is essential to balance plasmonic enhancement with the preservation of the tubular structure, which is critical for photocatalytic and photoelectrochemical applications. Excessive silver deposition compromises structural integrity and reduces active surface area, suggesting an optimal deposition window of approximately 10 minutes to achieve maximum catalytic performance [45].

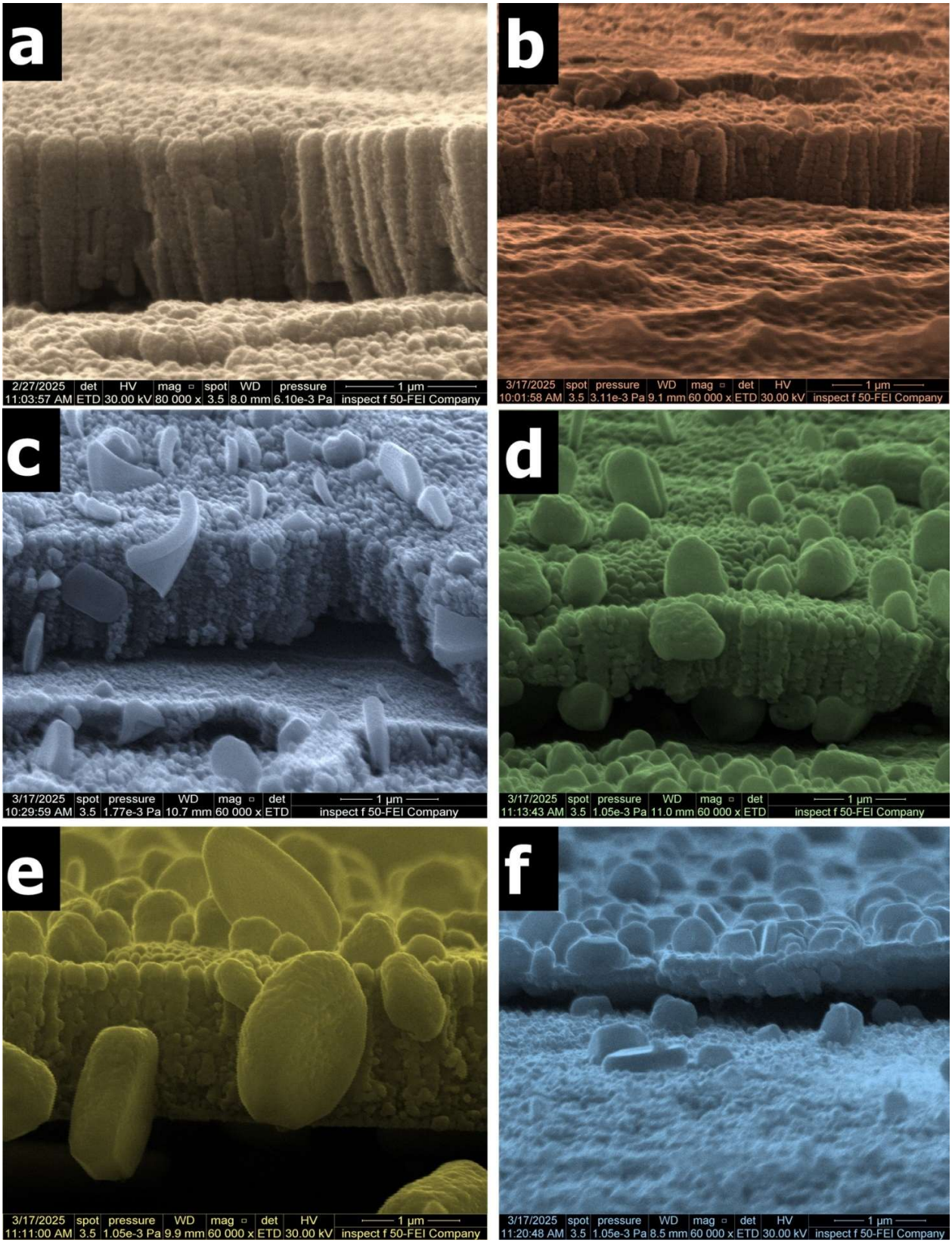

Figure 4. Cross-sectional images at various magnification of (a) pristine TiO_2 nanotube arrays (TNTs) and Ag-decorated TNTs obtained at various photodeposition durations: (b) Ag-5min@TNTs; (c) Ag-10min@TNTs; (d) Ag-15min@TNTs; (e) Ag-20min@TNTs; (f) Ag-25min@TNTs.

The EDS spectra shown in Figure 5a–f provide elemental characterization of pristine TiO_2 nanotube arrays and those decorated with silver (Ag) nanoparticles via photodeposition at various durations (5, 10, 15, 20, and 25 minutes). In Figure 5a (pristine TNTs), the spectrum confirms the presence of titanium (Ti) and oxygen (O), with Ti accounting for approximately 87.1 wt% and O for 12.9 wt%, consistent with the stoichiometry of TiO_2 and previous reports [46]. For Figure 5b (Ag-5min@TNT), a small Ag signal (0.4 wt%, 0.1 at%) is detected, indicating the onset of nanoparticle nucleation. At this early stage, Ag nanoparticles form sparse clusters or isolated particles due to the limited number of nucleation sites and the initial reduction of Ag^+ ions. In Figure 5c (Ag-10min@TNT), the Ag content slightly increases to 0.6 wt% (0.2 at%), reflecting initial nanoparticle growth and localized aggregation. Minor measurement variability may also contribute to this modest increase. Figure 5d (Ag-15min@TNT) shows a further rise in Ag content to 1.9 wt% (0.7 at%), indicating enhanced nucleation and more extensive surface coverage. This progressive accumulation suggests ongoing photoreduction and deposition, potentially leading to nanoparticle coalescence and increased density, consistent with reported photoreduction kinetics (Shinnur M et al., 2024) [47]. In Figure 5e (Ag-20min@TNT), Ag content increases substantially to 11.9 wt% (4.8 at%), corresponding to the formation of continuous or partially agglomerated nanoparticle layers. This stage, corroborated by FESEM images, significantly affects the optical and catalytic properties of the nanotube arrays. Finally, Figure 5f (Ag-25min@TNT) exhibits the highest Ag loading (19.7 wt%, 7.8 at%), associated with dense Ag nanoparticle agglomerates. While high Ag content can enhance photocatalytic activity and induce plasmonic effects, excessive deposition may result in

shadowing, particle sintering, and restricted reactant accessibility, potentially hindering performance. Overall, the EDS analysis demonstrates a clear time-dependent increase in Ag nanoparticles on TiO_2 nanotube arrays via photodeposition. The progressive Ag accumulation correlates with distinct morphological changes, particularly at longer deposition durations, highlighting a tunable strategy for optimizing surface functionality. These findings are in agreement with previous studies [48, 49].

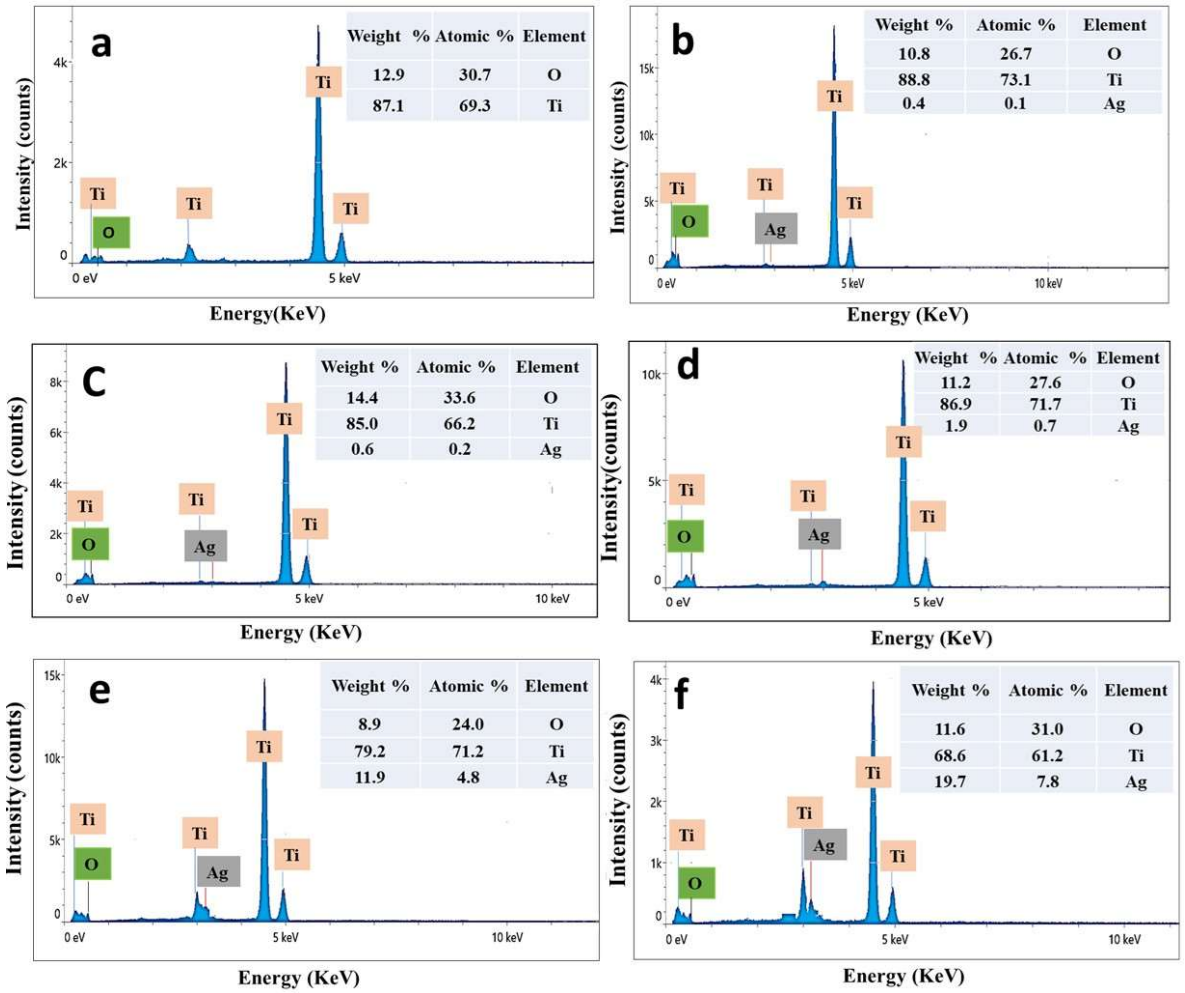

Figure 5. Energy-dispersive X-ray spectra of (a) pristine TiO_2 nanotube arrays (TNTs) and Ag-decorated TNTs obtained at various photodeposition durations: (b) Ag-5min@TNTs; (c) Ag-10min@TNTs; (d) Ag-15min@TNTs; (e) Ag-20min@TNTs; (f) Ag-25min@TNTs.

3.3 UV-Vis (DRS) analysis

As presented in Figure 6, the spectra provide valuable insight into the light-harvesting behavior of pristine TiO_2 nanotubes (TNTs) and their Ag-decorated counterparts synthesized via photodeposition at different time intervals. The pristine TiO_2 nanotubes (black curve) exhibit an absorption onset around 380 nm, corresponding to band gap energy of approximately 3.20 eV, which is consistent with the characteristic value of anatase TiO_2 that primarily absorbs ultraviolet light. The negligible absorption in the visible region (above 400 nm) highlights the limited solar utilization of pristine TiO_2, restricting its photocatalytic and photoelectrochemical performance.

Following Ag photodeposition, significant modifications in the optical response were observed. The absorption spectrum of Ag/ TiO_2 nanotubes exhibits a clear redshift compared to bare TiO_2, with the absorption onset moving from ~380 nm to ~460 nm, depending on the size and distribution of Ag nanoparticles. This redshift corresponds to an increase in the effective photon flux in the visible region, quantitatively enhancing the photogenerated charge density. For Ag-decorated samples obtained after 5 and 10 minutes of irradiation (red and blue curves), a distinct redshift of the absorption edge was detected, indicating the influence of silver nanoparticles through localized surface plasmon resonance (LSPR). Longer deposition durations (15 and 20 minutes, green and purple curves) resulted in broader absorption bands extending from 400 to 700 nm due to the increased Ag content, which enhances visible-light absorption via plasmonic excitation. At 25 minutes of deposition (yellow curve), a pronounced absorption peak appeared between 500 and 600 nm, characteristic of the LSPR of Ag nanoparticles. This plasmonic resonance originates from the collective oscillation of conduction electrons in Ag under light excitation, effectively extending the absorption range into the visible region.

However, excessive Ag loading (e.g., at 25 minutes) can lead to nanoparticle agglomeration, as clearly shown in the FESEM images (Figure 3), which induces light scattering and partial shielding effects, thereby diminishing photoelectrochemical efficiency. This observation emphasizes the importance of optimizing photodeposition duration to balance enhanced light absorption with uniform nanoparticle dispersion.

The optical band gaps (E_g) were estimated using the Tauc relation (Equation 2) [50]:

$$(\boldsymbol{\alpha h\nu})^{\boldsymbol{n}} = \boldsymbol{h\nu} - \boldsymbol{Eg} \qquad (2)$$

Where α is the absorption coefficient, $h\nu$ is the photon energy, and E_g is the optical band gap. $n = 2$ for direct band gap. The optical band gap (E_g) is determined by extrapolating the linear segment of the curve to zero. The band gap values obtained from the extrapolated linear regions of the Tauc plots are summarized in Table 1.

Table 1: The energy gap values of pristine TiO_2 nanotube arrays (TNTs) and Ag-decorated TNTs obtained at various photodeposition durations.

Constructions	Energy gap (eV)
TNTs	3.20
Ag-5 min/TNTs	2.80
Ag-10 min/TNTs	2.70
Ag-15 min/TNTs	2.86
Ag-20 min/TNTs	2.96
Ag-25 min/TNTs	3.05

As illustrated in Figure 7, the optical band gap decreases progressively with increasing Ag deposition time up to 10 minutes, reflecting enhanced visible-light absorption and improved charge transfer through metal–semiconductor interfacial interactions. The subsequent increase in

the apparent band gap beyond 15 minutes can be attributed to excessive Ag nanoparticle loading, leading to partial surface coverage and light shielding effects.

The observed modulation in optical properties arises from plasmonic and interfacial phenomena rather than intrinsic lattice modification as occurs in doping. Therefore, Ag decoration effectively tunes the optical response of TiO_2 nanotubes without altering their fundamental crystal structure. Consistent with these optical findings, photoelectrochemical measurements revealed a marked enhancement in photocurrent density for the optimally decorated TiO_2 nanotube arrays compared to pristine TiO_2. This improvement is primarily due to the synergistic influence of Ag-induced plasmonic enhancement and the formation of Schottky junctions, which facilitate electron extraction and suppress charge recombination at the TiO_2/electrolyte interface. Prolonged deposition (e.g., 25 minutes), however, resulted in decreased performance due to nanoparticle aggregation and scattering effects, in agreement with previously reported results [51, 52]. The Tauc analysis revealed a non-monotonic evolution of the apparent band gap with increasing Ag deposition time. The band gap decreased from 3.20 eV (pristine TNTs) to a minimum of ~2.70 eV at 10 min, coinciding with the formation of uniformly distributed and optimally sized Ag nanoparticles. This reduction is attributed to strong plasmon–semiconductor coupling, increased localized electromagnetic fields, and the introduction of shallow metal-induced states near the TiO_2 conduction band. However, at longer deposition times (15–25 min), the apparent band gap increased again (up to ~3.05 eV), which we associate with nanoparticle coalescence, loss of plasmonic resonance sharpness, and increased optical scattering. These effects weaken the near-field enhancement and reduce the contribution of Ag-induced sub-bandgap absorption, resulting in a partial reversal of the redshift observed at the optimal 10-minute deposition interval. This trend confirms that moderate Ag loading maximizes plasmonic enhancement, whereas excessive deposition deteriorates both the

optical response and the effective band-edge modulation. In the Ag-25/TiO_2 sample, the Tauc-derived band gap shows a slight decrease to 3.05 eV, while the DRS spectrum displays a strong absorption peak at ~620 nm. This peak originates from the localized surface plasmon resonance (LSPR) of Ag nanoparticles. The plasmonic absorption, along with mid-gap states and enhanced light scattering at high Ag loading, accounts for the mild redshift in the apparent band-gap edge, without indicating an actual narrowing of the intrinsic TiO_2 band gap.

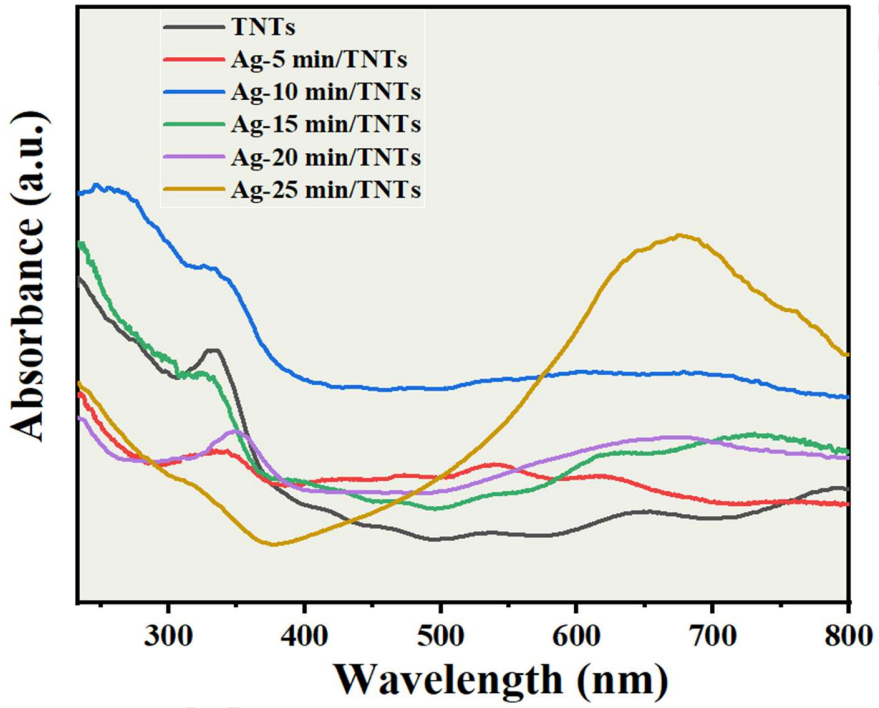

Figure 6. UV – Vis absorption spectra of pristine TiO_2 nanotube arrays (TNTs) and Ag-decorated TNTs obtained at various photodeposition durations.

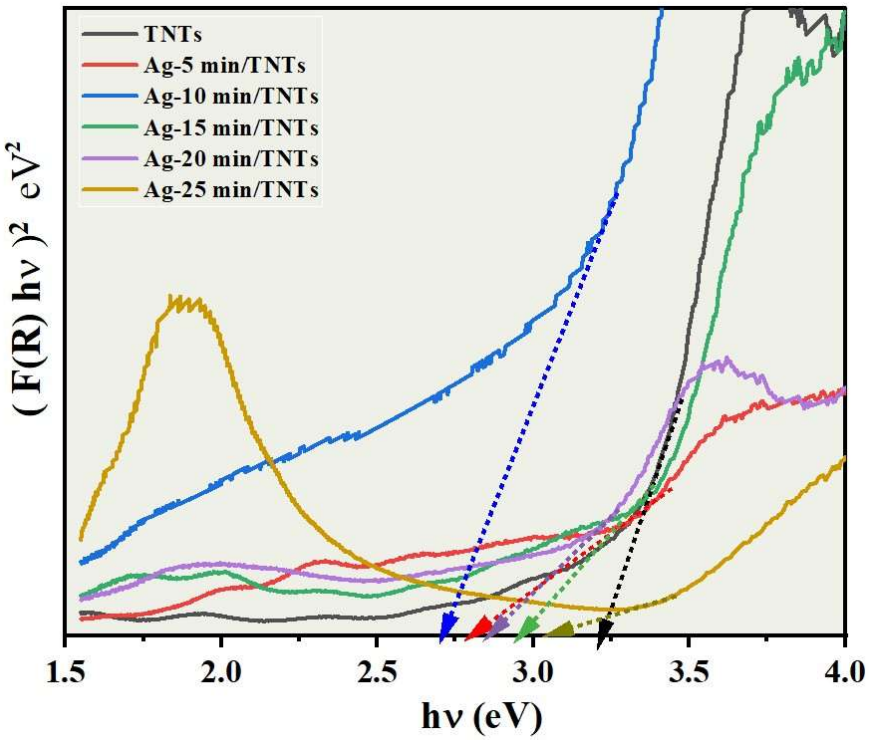

Figure 7. UV–Vis spectra bandgap energy curves of pristine TiO_2 nanotube arrays (TNTs) and Ag-decorated TNTs obtained at various photodeposition durations.

3.4 Photoelectrochemical Performance

Figure 8 presents the J–V characteristics evaluating the photoelectrochemical (PEC) performance of titanium dioxide (TiO_2) nanotubes (TNTs) synthesized via 1-hour anodization, before and after surface modification with silver (Ag) nanoparticles using photodeposition at various durations (5, 10, 15, 20, and 25 minutes). The photocurrent response under simulated solar irradiation was measured to assess the material's photoactivity and charge separation efficiency. Although complete triplicate datasets were not available, all photocurrent and efficiency measurements were repeated multiple times to verify stability and consistency. The results showed minimal variation under identical conditions, confirming the robustness of the observed trends. Pristine TNTs exhibited low photocurrent densities with a photoconversion efficiency of

0.18%. This limited performance is primarily due to the wide band gap (~3.2 eV), which restricts light absorption to the ultraviolet region, and the rapid recombination of photogenerated charge carriers in the TiO_2 matrix. Surface decoration with Ag nanoparticles significantly enhanced PEC performance. This improvement is mainly attributed to the surface plasmon resonance (SPR) effect of Ag nanoparticles, which extends light absorption into the visible spectrum and promotes effective charge separation. Ag nanoparticles act as electron sinks at the nanoscale, capturing photogenerated electrons and reducing the recombination rate a key factor in improving PEC efficiency.

Among the modified samples, Ag-10min@TNT exhibited the highest photocurrent density and photoconversion efficiency (0.39 mA/cm² and 0.48%, respectively), indicating an optimal Ag loading that balances light absorption enhancement and charge separation without introducing recombination centers. Few studies report photocurrent densities in Ag decorated TiO_2 systems. The only comparable report shows 0.35 mA/cm² using nanoplate morphology on an FTO substrate [48]. In contrast, our Ag-10 min/TiO_2 nanotube arrays on Ti foil achieve a higher photocurrent density of 0.39 mA/cm², corresponding to a photoconversion efficiency of 0.48%. This enhancement can be attributed to the one-dimensional nanotube morphology, which facilitates directional electron transport, reduces charge recombination, and increases the surface area available for Ag nanoparticle deposition. Shorter deposition times (5 min) resulted in insufficient Ag coverage, yielding lower SPR effects and moderate photocurrent (0.18 mA/cm², 0.22%). Conversely, longer deposition times (15, 20, and 25 min) led to excessive Ag accumulation and nanoparticle aggregation, which can block active sites, act as recombination centers, and hinder charge transfer. The corresponding photoconversion efficiencies were 0.20%,

0.19%, and 0.18% for 15, 20, and 25 min, respectively. Table 2 summarizes the photocurrent densities and photoconversion efficiencies.

Table 2: Photoconversion efficiency (η) of pristine TiO_2 nanotube arrays (TNTs) and Ag-decorated TNTs obtained at various photodeposition durations.

Sample	J_{ph} (mA/cm²) @ 0 V	η (%)
Pure TNTs	0.15	0.18
Ag-5 min/TNTs	0.18	0.22
Ag-10 min/TNTs	0.39	0.48
Ag-15 min/TNTs	0.17	0.20
Ag-20 min/TNTs	0.16	0.19
Ag-25 min/TNTs	0.15	0.18

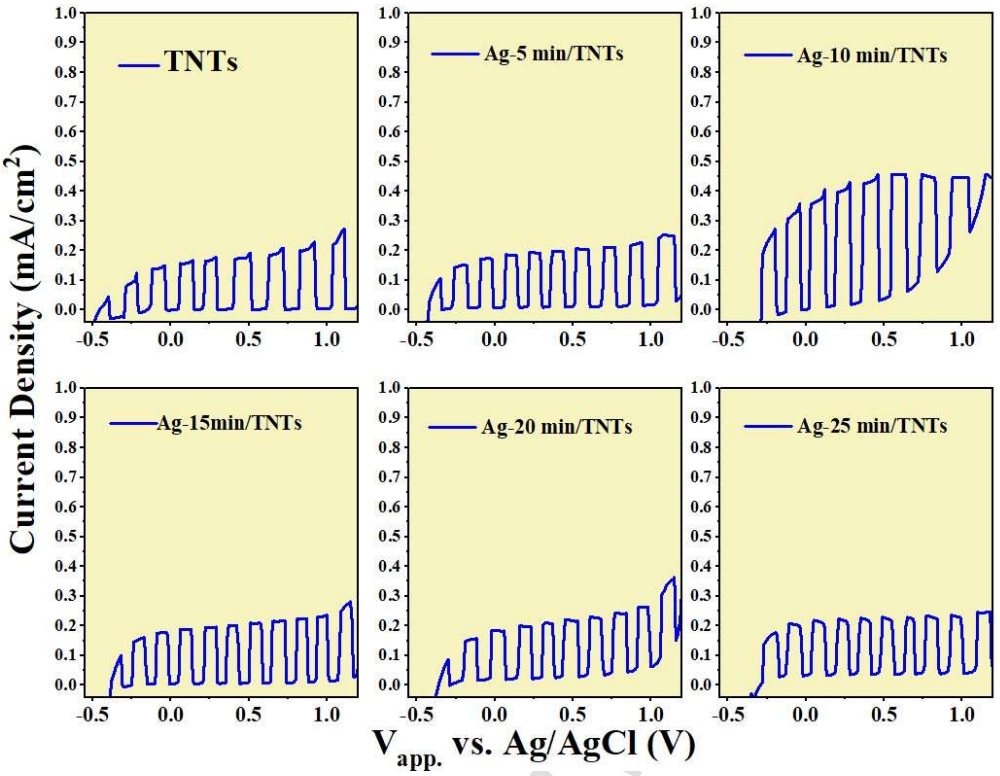

Figure 8. Linear sweep voltammograms obtained at the scan rate of 20 mV s^{-1} at applied potentials from –1 to 1 V under illumination intensity of 100 mW cm^{-2} in 0.1 M Na_2S and Na_2SO_3 electrolyte for plain of pristine TiO_2 nanotube arrays (TNTs) and Ag-decorated TNTs obtained at various photodeposition durations.

The valence and conduction band edges of TNTs and Ag-decorated TNTs were estimated using the following empirical relations [53]:

$$E_{CB} = \chi - E_o - 0.5E_g \quad (3)$$

$$E_{VB} = E_{CB} + E_g \quad (4)$$

where E_{CB} and E_{VB} are Conduction and valence band potentials (vs. NHE), χ is the electronegativity of TiO_2 (5.82 eV), E_o is the energy of free electrons on the hydrogen scale (4.5 eV) [54], and E_g is the band gap energy. It should be noted that the electronegativity-based calculation provides approximate band-edge estimation. The presence of surface-deposited Ag

nanoparticles does not alter the intrinsic electronegativity (χ = 5.82 eV) of TiO_2, but may introduce surface states and local electronic perturbations that are not captured by this empirical model.

Table 3: Band-edge positions (CB and VB) referenced to NHE and vacuum levels for pristine TiO_2 nanotube arrays and Ag-decorated TNTs synthesized at different photodeposition times.

Sample	Band Gap (eV)	CB Potential (V) vs. NHE	VB Potential (V) vs. NHE	ECB (eV) vs. Vac.	EVB (eV) vs. Vac.
TNTs	3.20	-0.28	+2.92	-4.78	-1.58
Ag-5 min/TNTs	2.80	-0.08	+2.72	-4.58	-1.78
Ag-10 min/TNTs	2.70	-0.03	+2.67	-4.53	-1.83
Ag-15 min/TNTs	2.86	-0.11	+2.75	-4.61	-1.75
Ag-20 min/TNTs	2.96	-0.16	+2.80	-4.66	-1.70
Ag-25 min/TNTs	3.05	-0.20	+2.84	-4.70	-1.65

Table 3 summarizes the band gap (E_g), conduction band edge potential (CB vs. NHE), and valence band edge potential (VB vs. NHE) for pristine titanium dioxide (TiO_2) nanotube (TNT) arrays and Ag-decorated TNTs prepared via photodeposition at different durations (5, 10, 15, 20, and 25 minutes). For Ag-modified samples, these values should be regarded as approximate, as metal-induced mid-gap states, interface dipoles, and surface plasmon–mediated electronic perturbations can shift the apparent band edges beyond the predictive capability of the empirical model [55]. Notably, Ag-10min@TNT shows a reduced optical band gap (2.70 eV) and an estimated ECB of −0.03 V vs. NHE (from −0.28 V for pristine TNTs), consistent with plasmon-driven band-edge modulation observed in Ag/TiO_2 heterostructures [56]. Although a less negative CB reduces the thermodynamic driving force for H^+ reduction, enhanced hot-electron injection and suppressed recombination at the Ag–TiO_2 interface can compensate kinetically [57]. The apparent increase in band gap at longer deposition times (≥15 min) is consistent with reports attributing such behavior to nanoparticle aggregation, light-scattering effects, and

modified surface states rather than intrinsic widening of TiO_2's band structure [58]. Overall, the results highlight the trade-off between band alignment and plasmonic/structural effects that governs the PEC response of Ag-decorated TNTs.

Figure 9 illustrates the charge transfer mechanism in the Ag@ TiO_2 NT heterostructure under visible-light illumination. Photon absorption excites electrons from the valence band (E_{VB}) to the conduction band (E_{CB}), generating holes in the valence band. Ag nanoparticles act as electron sinks due to Fermi level differences, efficiently capturing photogenerated electrons and suppressing electron–hole recombination. Electrons collected by Ag migrate through the external circuit to the counter electrode, reducing protons to generate hydrogen (H_2), while the remaining holes in TiO_2 oxidize water to produce oxygen (O_2) and additional protons. The required 1.23 V potential difference between H_2/H^+ and O_2/ H_2 O is maintained, enabling overall water splitting. The formation of a Schottky barrier at the Ag/TiO_2 interface is a key factor underlying the enhanced PEC performance observed in the Ag-decorated TiO_2 nanotube arrays. Using the reported electron affinity of TiO_2 (χ = 5.82 eV), the work-function mismatch between TiO_2 and Ag ($\Phi_{Ag} \approx$ 4.3–4.7 eV) creates a favorable energy offset that drives electron transfer from Ag to TiO_2 until Fermi-level equilibration is reached [59]. This electron redistribution induces downward band bending on the TiO_2 side, establishing a Schottky-like junction that promotes directional charge separation. Upon illumination, photogenerated electrons in TiO_2 readily migrate toward Ag nanoparticles, which act as electron sinks due to their lower Fermi level and high electrical conductivity [60]. This effectively suppresses electron–hole recombination, increasing the lifetime of photogenerated holes for oxidation reactions. These metallic bridges facilitate rapid electron transport from TiO_2 to Ag, effectively suppressing electron–hole recombination. As a result, the photoluminescence intensity of Ag-modified TiO_2 films is

reduced by more than half, consistent with the quenching behavior reported in Ref. [61]. Furthermore, Ag nanoparticles introduce localized surface plasmon resonance (LSPR), generating energetic ("hot") electrons that can be injected into the TiO_2 conduction band, further improving the separation and transport of photogenerated carriers. The combined action of plasmonic excitation and Schottky barrier-driven charge extraction accounts for the marked increase in photocurrent density after optimal Ag photodeposition.

In conclusion, controlling the Ag modification process is crucial for tuning band gaps, band edge potentials, and charge transfer efficiency. Optimizing deposition duration enhances visible-light absorption, promotes efficient charge separation, and improves hydrogen evolution, providing key insights for the design of nanostructured materials for renewable energy and photoelectrochemical applications [62-64].

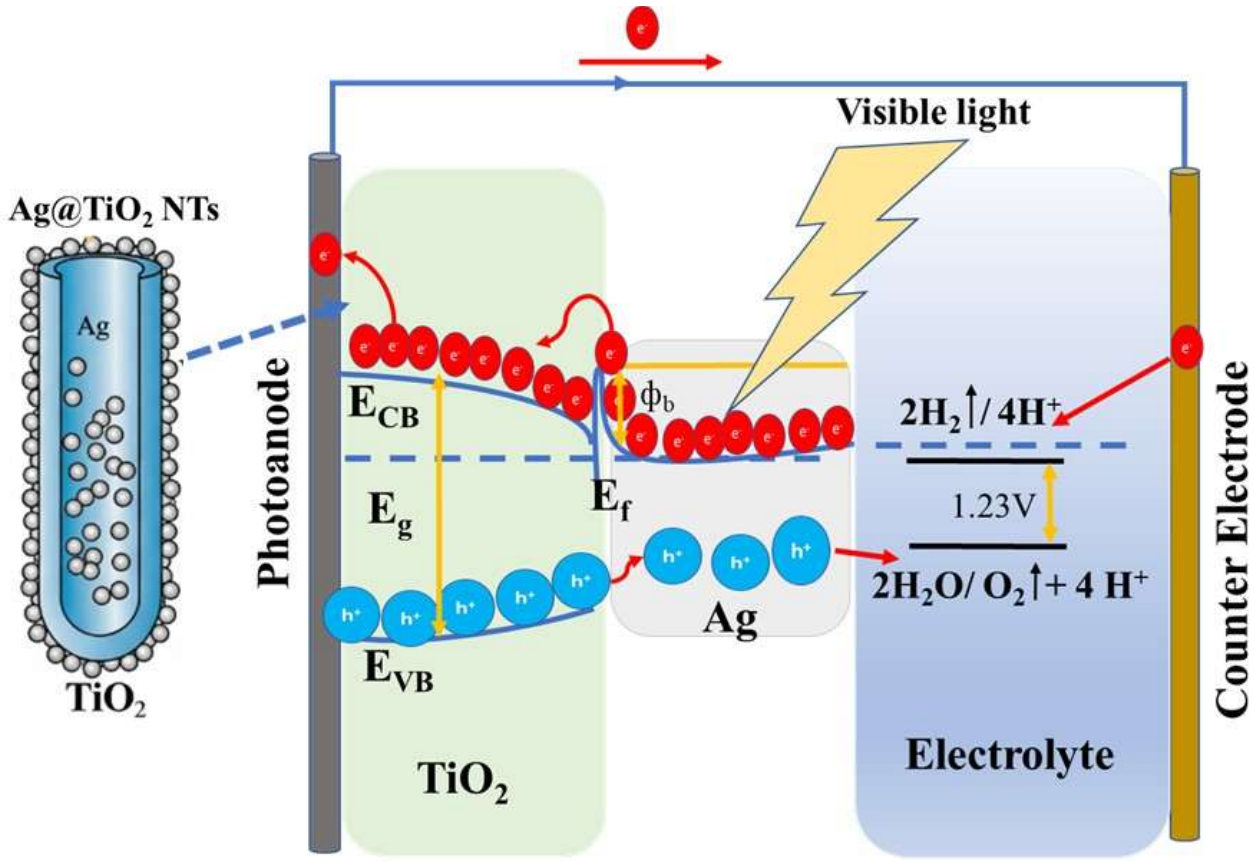

Figure 9. Schematic illustration of charge transfers in the Ag@TiO_2 nanotube heterostructure.

4. Conclusion

A time-controlled photoassisted deposition strategy was used to decorate TiO_2 nanotube arrays with Ag nanoparticles, enabling systematic tuning of their plasmonic and electronic behavior. The pristine TiO_2 NTs exhibited an inner diameter of ~95 nm, while early deposition stages (5–15 min) caused progressive wall thickening, reflected by increases in outer tube diameter from ~210 nm (5 min) to ~230 nm (10 min) and ~250 nm (15 min), despite the Ag particles not yet being visibly resolved. The photocurrent reached its maximum at 10 min, confirming that moderate Ag loading enhances charge separation while limiting recombination. At longer

deposition times, distinct Ag nanoparticles appeared, growing substantially from ~450 nm at 20 min to ~750 nm at 25 min, where excessive aggregation introduced recombination centers and reduced PEC performance. These results underscore the critical role of deposition time in controlling Ag nucleation, growth, and interface quality, offering clear design guidelines for optimizing plasmonic-semiconductor photoelectrochemical systems.

Acknowledgments

The authors gratefully acknowledge the support provided by the University of Al-Qadisiyah and the University of Kufa for facilitating this research. Their contribution in terms of laboratory access, technical support, and academic collaboration was instrumental in the successful completion of this study.

Data Availability Statement:

The data is contained within the article.

Conflict of interest

The authors declare no conflict of interest.

References

[1] Conte, R., Valentino, A., Romano, S., Yazdanpanah, S., Amrati, F. E. Z., Kandsi, F., Calarco, A. (2024). Microfluidic approach for the synthesis of silver nanoparticles as promising antimicrobial agent. *Int. J. Nano Dimens.,* 15(4): 32. https://doi.org/10.57647/j.ijnd.2024.1504.32

[2] Sohrabnezhad, S., Pourahmad, A., Sadjadi, M. S., Sadeghi, B. (2008). Nickel cobalt sulfide nanoparticles grown on AlMCM-41 molecular sieve. *Physica E*, 40(3): 684–688. https://doi.org/10.1016/j.physe.2007.09.081

[3] Sadeghi, B., Vahdati, R. A. R. (2012). Comparison and SEM-characterization of novel solvents of DNA/carbon nanotube. *Appl. Surf. Sci*., 258(7): 3086–3088. https://doi.org/10.1016/j.apsusc.2011.11.042

[4] Azari, B., Pourahmad, A., Sadeghi, B., Mokhtary, M. (2023). Green synthesis of SiO2 from Equisetum arvense plant for synthesis of SiO_2/ZIF-8 MOF nanocomposite as photocatalyst. *J. Coord. Chem*., 76(2): 219–231. https://doi.org/10.1080/00958972.2023.2166408

[5] Pourjafari, M., Ghane, M., Kaboosi, H., Sadeghi, B., Rezaei, A. (2022). Antibacterial properties of Ag–Cu alloy nanoparticles against multidrug-resistant Pseudomonas aeruginosa through inhibition of quorum sensing pathway and virulence-related genes. *J. Biomed. Nanotechnol*., 18(4): 1196–1204. https://doi.org/10.1166/jbn.2022.3331

[6] Khodadad, H., Hatamjafari, F., Pourshamsian, K., & Sadeghi, B. (2021). Microwave-assisted synthesis of novel pyrazole derivatives and their biological evaluation as anti-bacterial agents. *Comb. Chem. High Throughput Screen*., 24(5): 695–700. https://doi.org/10.2174/1386207323666201019152206

[7] Al-Jawad, S. M., Mohammad, M. R., & Imran, N. J. (2018). Effect of electrolyte solution on structural and optical properties of TiO_2 grown by anodization technique for photoelectrocatalytic application. *Surface Review and Letters*, *25*(04):1850078. https://doi.org/10.1142/S0218625X18500786

[8] Singh, J., Juneja, S., Soni, R. K., & Bhattacharya, J. (2021). Sunlight mediated enhanced photocatalytic activity of TiO_2 nanoparticles functionalized CuO-Cu_2O nanorods for removal of methylene blue and oxytetracycline hydrochloride. *Journal of Colloid and Interface Science*, *590*, 60-71. https://doi.org/10.1016/j.jcis.2021.01.022

[9] Singh, J., & Soni, R. K. (2020). Fabrication of hydroxyl group-enriched mixed-phase TiO2 nanoflowers consisting of nanoflakes for efficient photocatalytic activity. *Journal of Materials Science: Materials in Electronics*, *31*(15), 12546-12560. https://doi.org/10.1007/s10854-020-03805-w

[10] Saleh, H. M., Hassan, A. I. (2024). The challenges of sustainable energy transition: A focus on renewable energy. *Appl. Chem. Eng.*, 7: 2084. https://doi.org/10.59429/ACE.V7I2.2084

[11] Al-Jawad, S. M., Mohaisen, R. S., Imran, N. J., Mohammad, M. R., Alhusseiny, A., & Alhusseiny, I. M. (2024) Structural, Morphological, and Optical Properties of TiO_2/CdS Core-Shell System Prepared by Two Method for Photoelectrocatalytic Application. In *Journal of Physics: Conference Series* 2857(1): 012052. https://doi.org/10.1088/1742-6596/2857/1/012052

[12] Al-Jawad, S. M., Imran, N. J., & Mohammad, M. R. (2020). Effect of electrolyte solution and deposition methods on TiO2/CdS core–shell nanotube arrays for photoelectrocatalytic application. *The European Physical Journal Applied Physics*, *92*(2): 20102. https://doi.org/10.1051/epjap/2020200127

[13] Singh, J., & Soni, R. K. (2021). Efficient charge separation in Ag nanoparticles functionalized ZnO nanoflakes/CuO nanoflowers hybrids for improved photocatalytic and SERS activity. Colloids and Surfaces A: Physicochemical and Engineering Aspects, 626: 127005. https://doi.org/10.1016/j.colsurfa.2021.127005

[14] Vikrant, K., Weon, S., Kim, K. H., Sillanpää, M. (2021). Platinized titanium dioxide (Pt/TiO_2) as a multi-functional catalyst for thermocatalysis, photocatalysis, and photothermal catalysis for removing air pollutants. *Appl. Mater. Today*, 23: 100993. https://doi.org/10.1016/J.APMT.2021.100993

[15] Singh, J., & Soni, R. K. (2021). Tunable optical properties of Au nanoparticles encapsulated TiO2 spheres and their improved sunlight mediated photocatalytic activity. *Colloids and Surfaces A: Physicochemical and Engineering Aspects*, 612: 126011.https://doi.org/10.1016/j.colsurfa.2020.126011

[16] Zarzzeka, C., Goldoni, J., Lenzi, G. G., Bagatini, M. D., & Colpini, L. M. S. (2024). Photocatalytic action of Ag/TiO2 nanoparticles to emerging pollutants degradation: a comprehensive review. *Sustainable Chemistry for the Environment*, *8*: 100177. https://doi.org/10.1016/j.scenv.2024.100177

[17] Obaiah, G. O., Kemparajegowda, J., Gireesha, J., & Mylarappa, M. (2023). Comparative study of TiO2 and palladium doped TiO2 nano catalysts for water purification under solar and ultraviolet irradiation. Chem. Inorg. Mater., 1: 100002. https://doi.org/10.1016/J.CINORG.2023.100002.

[18] Lee, S. H., & Jun, B. H. (2019). Silver nanoparticles: Synthesis and application for nanomedicine. Int. *J. Mol. Sci*., 20: 865. https://doi.org/10.3390/IJMS20040865

[19] Jain, P. K., Huang, X., El-Sayed, I. H., & El-Sayed, M. A. (2008). Noble metals on the nanoscale: Optical and photothermal properties and applications. Accounts of Chemical Research, 41(12), 1578–1586. https://doi.org/10.1021/ar7002804

[20] Xing, M., Xu, W., Dong, C., Bai, Y., Zeng, J., Zhou, Y., & Zhang, J. (2016). *Metal plasmonic TiO_2 photocatalysis*. Chemical Reviews, 116(19), 10292–10334. https://doi.org/10.1021/acs.chemrev.5b00714.

[21] Zhang, Z., Zhang, L., Hedhili, M. N., Zhang, H., & Wang, P. (2013). *Plasmonic gold nanocrystals coupled with UV photocatalytic semiconductors for visible-light generation of reactive oxygen species*. ACS Nano, 7(5), 4537–4544. https://doi.org/10.1021/nn401585v.

[22] Cheng, X., Yu, X., Xing, Z., Yang, L., & Chen, Z. (2020). Ag-decorated TiO_2 nanotube arrays for enhanced photoelectrochemical water splitting. Applied Surface Science, 507, 145067. https://doi.org/10.1016/j.apsusc.2019.145067

[23] Nanda, B. P., Rani, P., Paul, P., Aman, S. S., Ganti, S. S., Bhatia, R. (2024). Recent trends and impact of localized surface plasmon resonance (LSPR) and surface-enhanced Raman spectroscopy (SERS) in modern analysis. *J. Pharm. Anal*., 14: 100959. https://doi.org/10.1016/J.JPHA.2024.02.013

[24] Zhao, W., Ma, W., Chen, C., Zhao, J., & Shuai, Z. (2004). Efficient degradation of toxic organic pollutants with Ag@TiO_2 under visible irradiation. *Journal of the American Chemical Society*, 126(15), 4782–4783. https://doi.org/10.1021/ja039718w.

[25] A Liu, W., Cheng, H., Xu, Y., Zheng, R., & Chen, Z. (2019). Plasmon-enhanced photoelectrochemical performance of Ag/TiO_{2-x} nanotube arrays prepared by electrodeposition and thermal treatment. *Electrochimica Acta, 298*: 280–289. https://doi.org/10.1016/j.electacta.2018.12.123

[26] Zhang, Y., Kong, L., Xia, L., & Wang, S. (2020). Tuning plasmonic behavior of TiO_2 nanotubes by controlled photodeposition of Ag and Au nanoparticles. *Nanoscale Advances, 2*(5): 2152–2160. https://doi.org/10.1039/D0NA00123A.

[27] Veziroglu, S., Shondo, J., Tjardts, T., Sarwar, T. B., Sünbül, A., Mishra, Y. K., & Aktas, O. C. (2024). Photocatalytic deposition of noble metals on 0D, 1D, and 2D TiO2 structures: a review. Nanoscale Advances, 6(24): 6096-6108. https://doi.org/10.1039/d4na00623b.

[28] Yang, F., Li, Q., Sun, J., & Zhang, L. (2021). Plasmon-enhanced photocatalytic activity of Ag-decorated TiO_2 tube-in-tube fibers. *Journal of Materials Chemistry A, 9*(12): 7424–7433. https://doi.org/10.1039/D0TA11782D.

[29] Chen, X., Li, Y., Wang, Z., & Zhao, J. (2022). Surface-enhanced Raman scattering activity of TiO_2 decorated with dense Ag nanoparticles. *Applied Surface Science, 573*: 151607. https://doi.org/10.1016/j.apsusc.2021.151607.

[30] Holi, A. M., Zainal, Z., Ayal, A. K., Chang, S. K., Lim, H. N., Talib, Z. A., & Yap, C. C. (2018). Effect of heat treatment on photoelectrochemical performance of hydrothermally synthesised Ag2S/ZnO nanorods arrays. Chemical Physics Letters, 710: 100-107. https://doi.org/10.1016/j.cplett.2018.08.069

[31] Rostas, A. M., Suciu, R. C., Roşu, M. C., Turza, A., Cosma, D. V., Tripon, S., Fort, C. I., Danciu, V., Baia, M., Bocirnea, A., & Indrea, E. (2025). Annealing temperature, a key factor in shaping Ag-decorated TiO2 aerogels as efficient visible-light photocatalysts. *Mater. Chem. Phys*., 337: 130557. https://doi.org/10.1016/J.MATCHEMPHYS.2025.130557

[32] Soliman, K. A., Zedan, A. F., & Khalifa, A. (2017). Silver nanoparticles-decorated titanium oxynitride nanotube arrays for enhanced solar fuel generation. *Sci. Rep*., 7: 1913. https://doi.org/10.1038/s41598-017-02124-1

[33] Jamali, S., Moshaii, A., Mohammadi, K. (2019). Optimization of Ag loaded TiO. Iranian J. Hydrogen Fuel Cell, 2: 133–140. https://doi.org/10.22104/ijhfc.2019.3715.1193

[34] Lian, Z., Wang, W., Xiao, S., Li, X., Cui, Y., Zhang, D., Li, G., Li, H. (2015). Plasmonic silver quantum dots coupled with hierarchical TiO2 nanotube arrays photoelectrodes for efficient visible-light photoelectrocatalytic hydrogen evolution. *Sci. Rep*., 5: 10461. https://doi.org/10.1038/srep10461

[35] Chakhtouna, H., Benzeid, H., Zari, N., Qaiss, A.E.K., Bouhfid, R. (2021). Recent progress on Ag/TiO2 photocatalysts: Photocatalytic and bactericidal behaviors. *Environ. Sci. Pollut. Res*., 28: 44638–44666. https://doi.org/10.1007/S11356-021-14996-Y.

[36] Dávila-Martínez, R.E., Cueto, L.F., Sánchez, E.M. (2006). Electrochemical deposition of silver nanoparticles on TiO2/FTO thin films. *Surf. Sci*., 600: 3427–3435. https://doi.org/10.1016/J.SUSC.2006.06.041

[37] Ivanova, T., Harizanova, A., Koutzarova, T., Closset, R. (2024). Crystallization and optical behaviour of nanocomposite sol-gel TiO_2:Ag films. *Molecules*, 29: 5156. https://doi.org/10.3390/MOLECULES29215156

[38] Ali, I., Suhail, M., Alothman, Z.A., Alwarthan, A. (2018). Recent advances in syntheses, properties and applications of TiO2 nanostructures. RSC Adv., 8: 30125–30147. https://doi.org/10.1039/C8RA06517A

[39] Wang, D., Zhou, F., Liu, Y., Liu, W. (2008). Synthesis and characterization of anatase TiO2 nanotubes with uniform diameter from titanium powder. *Mater. Lett*., 62: 1819–1822. https://doi.org/10.1016/J.MATLET.2007.10.011

[40] Nycz, M., Arkusz, K. (2025). From nano- to microsilver: Morphology control and shape evolution of facile one-step electrochemical synthesis of silver particles on TiO_2 nanotubes.

Langmuir, 13: 52. https://doi.org/10.1021/ACS.LANGMUIR.5C01022/SUPPL_FILE/LA5C01022_SI_001.PDF

[41] Rabah, M.A., Girgis, N.N. (2022). Mechanism of silver nanoparticles deposition by electrolysis and electroless methods on a graphite substrate. *Int. J. Nonferrous Metall*., 10: 1–14. https://doi.org/10.4236/IJNM.2022.101001

[42] Lincho, P., Mazierski, T., Klimczuk, T., Martins, R.C., Gomes, J., Zaleska-Medynska, A. (2024). TiO2 nanotubes modification by photodeposition with noble metals: Characterization, optimization, photocatalytic activity, and by-products analysis. *J. Environ. Chem. Eng*., 12: 112990. https://doi.org/10.1016/J.JECE.2024.112990

[43] Chakhtouna, H., Benzeid, H., Zari, N., Qaiss, A.E.K., Bouhfid, R. (2021). Recent progress on Ag/TiO2 photocatalysts: Photocatalytic and bactericidal behaviors. *Environ. Sci. Pollut. Res*., 28: 44638–44666. https://doi.org/10.1007/S11356-021-14996-Y

[44] Taipina, M.O., de Mello, M.G., Tamborlin, L., Pereira, K.D., Luchessi, A.D., Cremasco, A., Caram, R. (2021). A novel Ag doping Ti alloys route: Formation and antibacterial effect of the TiO_2 nanotubes. *Mater. Chem. Phys*., 261: 124192. https://doi.org/10.1016/j.matchemphys.2020.124192

[45] Xu, J., Liu, Y., & Zhao, Y. (2020). Effect of Ag loading position on the photocatalytic performance of TiO2 nanocolumn arrays. Beilstein Journal of Nanotechnology, 11(1): 717-728. https://doi.org/10.3762/bxiv.2019.110.v1

[46] Ayal, A.K. (2019). Effect of anodization duration in the TiO_2 nanotubes formation on Ti foil and photoelectrochemical properties of TiO_2 nanotubes. Al-Mustansiriyah J. Sci., 29: 77–81. https://doi.org/10.23851/mjs.v29i3.640

[47] Shinnur, M.V., Menegazzo, M., Bussetti, G., Duò, L., Pedeferri, M.P., Diamanti, M.V. (2024). Studying the photoactivity of Ag-decorated TiO_2 nanotubes with combined AFM and Raman spectroscopy. *Surfaces*, 7: 938–950. https://doi.org/10.3390/SURFACES7040061

[48] Zheng, X., Zhang, D., Gao, Y., Wu, Y., Liu, Q., Zhu, X. (2019). Synthesis and characterization of cubic Ag/TiO2 nanocomposites for the photocatalytic degradation of methyl orange in aqueous solutions. *Inorg. Chem. Commun.*, 110: 107589. https://doi.org/10.1016/J.INOCHE.2019.107589

[49] Trabelsi, K., Hajjaji, A., Gaidi, M., Bessais, B., El Khakani, M.A. (2017). Enhancing the photoelectrochemical response of TiO_2 nanotubes through their nanodecoration by pulsed-laser-deposited Ag nanoparticles. *J. Appl. Phys*., 122: 154737. https://doi.org/10.1063/1.4998439

[50] Klein, J., Kampermann, L., Mockenhaupt, B., Behrens, M., Strunk, J., & Bacher, G. (2023). Limitations of the Tauc plot method. Advanced Functional Materials, 33(47) :2304523. https://doi.org/10.1002/adfm.202304523

[51] Peerakiatkhajohn, P., Yun, J. H., Butburee, T., Nisspa, W., & Thaweesak, S. (2022). Surface plasmon-driven photoelectrochemical water splitting of a Ag/TiO 2 nanoplate photoanode. *RSC advances*, *12*(5), 2652-2661. https://doi.org/10.1039/d1ra09070d

[52] Nycz, M., Arkusz, K., & Pijanowska, D. G. (2019). Influence of the silver nanoparticles (AgNPs) formation conditions onto titanium dioxide (TiO2) nanotubes based electrodes on their impedimetric response. *Nanomaterials*, *9*(8), 1072. https://doi.org/10.3390/nano9081072

[53] Holi, A. M., Zainal, Z., Talib, Z. A., Lim, H. N., Yap, C. C., Chang, S. K., & Ayal, A. K. (2017). Enhanced photoelectrochemical performance of ZnO nanorod arrays decorated with CdS shell and Ag2S quantum dots. Superlattices and Microstructures, 103: 295-303. http://dx.doi.org/10.1016/j.spmi.2017.01.035

[54] Abdullah, E.A. (2019). Band edge positions as a key parameter to a systematic design of heterogeneous photocatalyst. *Eur. J. Chem*., 10: 82–94. http://orcid.org/0000-0001-9698-6203

[55] Makuła, P., Pacia, M., Macyk, W. (2018). How to correctly determine the band gap energy of modified semiconductor photocatalysts based on UV-Vis spectra. *J. Phys. Chem. Lett*., 9: 6814–6817. https://doi.org/10.1021/ACS.JPCLETT.8B02892

[56] Mills, A., Halfpenny, P.J., Stewart, M., Faulds, K., Robertson, P., Hodgen, S., Smith, W.E., Graham, D., Hill, G. (2004). Characterization of novel Ag on TiO_2 films for surface-enhanced Raman scattering. Appl. Spectrosc., 58: 922–928. https://opg.optica.org/abstract.cfm?uri=as-58-8-922

[57] Song, J., Long, J., Liu, Y., Xu, Z., Ge, A., Piercy, B.D., Cullen, D.A., Ivanov, I.N., McBride, J.R., Losego, M.D., Lian, T. (2021). Highly efficient plasmon induced hot-electron transfer at Ag/TiO_2 interface. *ACS Photonics*, 8: 1497–1504. https://doi.org/10.1021/ACSPHOTONICS.1C00321

[58] Fu, C., Liu, L., Zhao, G. (2024). Role of Ag loading on the concentration of surface-reaching photoexcited holes in TiO_2 nanoparticles. *J. Phys. Chem. C*, 128: 810–818. https://doi.org/10.1021/acs.jpcc.3c07203

[59] Tian, Y., & Tatsuma, T. (2005). Mechanisms and applications of plasmon-induced charge separation at TiO_2 films loaded with gold nanoparticles. *Journal of the American Chemical Society*, *127*(20): 7632-7637. https://doi.org/10.1021/ja042192u

[60] Marcos P.C. da Silva, Aldo M.C. Gomes, Adhimar F. Oliveira, Danilo R. Huanca (2024). Enhanced Schottky barrier engineering in silver-doped TiO2/p-Si heterojunctions: Insights into electrical behavior and charge carrier dynamics. *Materials Chemistry and Physics*, 328: 129995. https://doi.org/10.1016/j.matchemphys.2024.129995

[61] Fang, M., Liu, F., Li, T., Zhang, W., Xia, H., Rao, K. V., & Belova, L. (2019). Inkjet printing Ag-TiO2 thin films with suppressed photoluminescence. *Semiconductor Science and Technology*, *34*(10), 105027. https://doi.org/10.1088/1361-6641/ab3d77

[62] Helal, A., Harraz, F.A., Ismail, A.A., Sami, T.M., Ibrahim, I.A. (2017). Hydrothermal synthesis of novel heterostructured $Fe2O_3/Bi_2S_3$ nanorods with enhanced photocatalytic activity under visible light. *Appl. Catal. B*, 213: 18–27. https://doi.org/10.1016/J.APCATB.2017.05.009

[63] Guo, M., Du, J. (2012). First-principles study of electronic structures and optical properties of Cu, Ag, and Au-doped anatase TiO_2. *Physica B*, 407: 1003–1007. https://doi.org/10.1016/j.physb.2011.12.128

[64] Perini, J.A.L., Torquato, L.D.M., Irikura, K., Zanoni, M.V.B. (2019). Ag/polydopamine-modified Ti/TiO_2 nanotube arrays: A platform for enhanced CO_2 photoelectroreduction to methanol. *J. CO_2 Util*., 34: 596–605. https://doi.org/10.1016/j.jcou.2019.08.006